

A revision of the vdB 130 cluster stellar content based on GAIA DR2 Data. Interstellar extinction toward the Cyg OB1 supershell.

T.G. Sitnik^{1*}, A.S. Rastorguev^{1,2†}, A.A. Tatarnikova¹, A.M. Tatarnikov¹,
O.V. Egorov¹, A.A. Tatarnikov²

¹ Lomonosov Moscow State University, Sternberg Astronomical Institute, Universitetsky pr. 13, Moscow 119234, Russia

² Lomonosov Moscow State University, Faculty of physics, Leninskie Gory 1 b.2, Moscow 119992, Russia

Accepted 2020 August 28. Received 2020 August 07; in original form 2020 May 02

ABSTRACT

Two star-forming regions are studied: the young embedded open cluster vdB 130 and the protocluster neighbourhood observed in the head and tail of the cometary molecular cloud located in the wall of the expanding supershell surrounding the Cyg OB1 association. The GAIA DR2 catalogue is employed to verify the stellar composition of the vdB 130 cluster whose members were earlier selected using the UCAC4 catalogue. The new sample of vdB 130 members contains 68 stars with close proper motions (within 1 mas yr^{-1}) and close trigonometric parallaxes (ranging from 0.50 to 0.70 mas). The relative parallax error is shown to increase with distance to objects and depend on their magnitude. At a distance of 1.5–2 kpc it is of about 3–7 per cent and 20–30 per cent for bright and faint stars, respectively. The cluster is not older than ~ 10 Myr. New spectroscopic and photometric observations carried out on Russian telescopes are combined with GAIA DR2 to search for optical components in the protocluster region – a new starburst. An analysis of 20 stars in the vicinity of the protocluster revealed no concentration of either proper motions or parallaxes. According to spectroscopic, photometric, and trigonometric estimates, the distances to these stars range from 0.4 to 2.5 kpc, and colour excess is shown to increase with a distance D (kpc) in accordance with the law: $E(B - V) \simeq 0.6 \times D \text{ mag}$.

Key words: open clusters and associations: individual: vdB 130 – dust, extinction – stars: distances – ISM: clouds – infrared: ISM reddening – stars: protostars

1 INTRODUCTION

Nowadays it is well established that star formation could be regulated by many factors like turbulence, feedback from outflows, supernova explosions and expanding HII regions (e.g., see review by Elmegreen 1998, 2010). These and other factors work together sculpting a fine structure of molecular clouds with filaments, pillars, blobs, peppered with young stellar objects (YSOs) in the rims of expanding bubbles. A growing number of observational works supports the idea of sequential and triggering star formation on both local and global scales (e.g., Zavagno et al. 2006; Deharveng et al. 2010; Dale et al. 2015; Egorov et al. 2017, among many others). Given complexity of the process, along with large-scale studies, a detailed look at some specific objects and regions

can be useful for distinguishing between general and particular features of the star formation process.

The aim of this work is to continue the study of star formation regions in the walls of an expanding supershell formed by the wind and the UV radiation of stars in the Cyg OB1 association. We present an investigation of the stellar content of the cluster vdB 130 and of optical counterparts of the protocluster using the new catalogue GAIA DR2 (Gaia Collaboration 2018¹).

We have already partially studied the region of ongoing star formation in the supershell related to the cometary molecular cloud (pillar) (Sitnik et al. 2015, 2019, hereinafter referred to as Paper I and Paper II, and Tatarnikova et al. 2016). This region ($\alpha = 20^{\text{h}}16^{\text{m}} - 20^{\text{h}}18^{\text{m}}$, $\delta = 39^{\circ}15' - 39^{\circ}30'$) resides in the wall of the expanding supershell

* E-mail: tat.sitnik2011@yandex.ru

† E-mail: alex.rastorguev@gmail.com

¹ VizieR On-line Data catalogue: I/345/gaia2

surrounding the Cyg OB1 stellar association (Fig.1,top). The Cyg OB1 association includes at least 50 OB stars (Humphreys & McElroy 1984). The size of the supershell driven by this association is $3^\circ \times 4^\circ$. In the supershell region mentioned above a cometary molecular cloud is observed (Schneider et al. 2007). It is associated with two sites of star formation: the young embedded cluster vdB 130 in the head and a compact protocluster in the tail (Fig.1, bottom). We found this protocluster in a dense condensation of the cloud and described it in Paper II (see fig. 11 in Paper II). The cloud is extended toward the illuminating source, i.e., toward the nearest OB stars of the Cyg OB1 association. The molecular cloud has a size of 0.4 degrees or 12 pc at the adopted distance of 1.8 ± 0.3 kpc to the cluster and association. The vdB 130 cluster has 44 members selected based on UCAC4 proper motions. They are listed in table 2 in Paper I. The physical connection of the Cyg OB1 association, supershell, and vdB 130 cluster, and the cloud follows from the distance estimates, measured radial velocities, and a number of indirect factors (Paper I). The age of vdB 130 was estimated as 5–10 Myr. According to near-IR data, the true distance modulus to the cluster, its minimum colour excess, and distance are equal to $(K - M_{Ks}) = 11.26 \pm 0.30$ mag, $E(J - H) = 0.27 \pm 0.02$ mag, and about 1.8 kpc, respectively. The interstellar extinction law inside the cluster region differs significantly from the normal law, with $R_v = A_v/E(B - V)$ reaching values of 6–8. On the other hand, the normal law is valid in front of the cluster (Tatarnikova et al. 2016). Some cluster stars are located in the centres of dust clumps inside the IR shell.

We use the data from GAIA DR2 (Gaia Collaboration 2018) to analyse the star membership in two groupings in the supershell surrounding the Cyg OB1 association – in the cluster vdB 130 and in the protocluster. The embedded cluster vdB 130 was initially identified by Racine (1974) as a group of 14 B-type stars. We added another 30 stars with close proper motions from the UCAC4 catalogue (in terms of the accuracy of the UCAC4 catalogue) (Paper I). However, the GAIA DR2 catalogue allows us to appreciably refine the selection of stars both by proper motions and distances. It is especially important for objects observed toward the Cygnus arm, because the proper motions due to the differential rotation of the Galaxy vary slightly with distance.

We also performed optical and infrared photometric and spectroscopic observations on Russian telescopes in order to clarify the spectral classification of stars, study the spectral energy distribution, and estimated the value of interstellar extinction.

In this paper we use new observational data, as well as archival data from the GAIA DR2 catalogue in order to verify the vdB 130 cluster earlier studied using UCAC4 proper motions and search for possible optically visible member stars of the protocluster. We use our data to study interstellar extinction toward the supershell formed by Cyg OB1 stars. Section 2 describes the instruments and data reduction process employed for spectroscopic and photometric observations. Section 3 analyses the line-of-sight distribution of vdB 130 stars and potential members of the optical component of the protocluster (using GAIA DR2 catalogue). In the same section we estimated the age of the cluster using stars with a known spectral classification (Tatarnikova et al. 2016). Section 4 presents the results of the spectral clas-

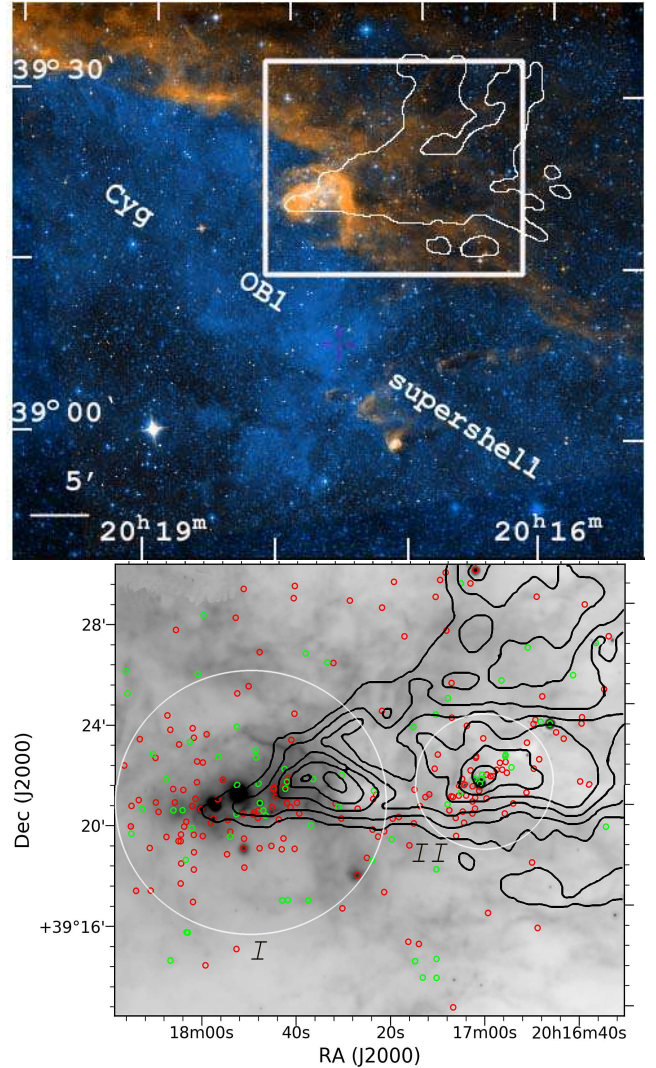


Figure 1. Northwestern part of the supershell surrounding the stellar association Cyg OB1. Top: superimposed images of the optical (blue) and IR (red) maps (the latter is based on 5.8- μm *Spitzer* data) and the contour delimiting the molecular cloud (Schneider et al. 2007). Bottom: zoomed-in 24- μm image of the region in the rectangle shown in the top panel. The circles mark the cluster vdB130 (I) and protocluster (II) regions. The green and red circles indicate type I and II protostars, respectively (see Paper II). Isocontours describe the molecular cloud mentioned above.

sification of stars seen toward the protocluster and colour excess estimates. In section 5 interstellar extinction toward the cometary molecular cloud is analysed using GAIA DR2 results among other data. Section 6 summarizes the results of the study.

2 OBSERVATIONS AND DATA REDUCTION.

This study is based on optical and near-IR observations performed with the 6-m telescope of Special Astrophysical Observatory of Russian Academy of Sciences (SAO RAS), 2.5-m telescope of Caucasian Mountain Observatory of Sternberg Astronomical Institute of M.V. Lomonosov Moscow

Table 1. Log of observations.

Instrument	Slit/filters (stars)	Date	$T_{\text{exp, s}}$	$\theta, ''$
SCORPIO	#1 (6, 7, 12, 23)	2017 Jul 28	180	1.8
SCORPIO	#2 (2,9,17, 22)	2017 Jul 28	240	1.8
SCORPIO	#3 (5, 13)	2017 Jul 28	180	1.5
SCORPIO	#4 (3, 8, 10)	2017 Jul 28	1320	1.5
SCORPIO	#5 (15, 19, 21)	2017 Jul 30	1800	3.0
SCORPIO	#6 (11, 18)	2017 Jul 31	1200	3.0
SCORPIO	#7 (13, 14, 20)	2017 Jul 31	791	3.0
ASTRONIRCAM	<i>JHK</i>	2016 Sep 17	40	0.8
CCD photometer	<i>BVR_c</i>	2018 Aug 05	600	1.2

State University (SAI MSU) and 60-cm telescope of the Crimean Astronomical Station of SAI MSU. The archival data obtained with *Spitzer* and *GAIA* (DR2) space observatories were also used. Below we present a description of the observations and data reduction. The log of our observations is given in Table 1, where the exposure time, T_{exp} , the field of view (FOV), the final angular resolution, θ , the final spectral resolution, $\delta\lambda$, and the bandwidth (FWHM) of the used filter are indicated.

2.1 Spectroscopic observations and data reduction.

Spectroscopic observations on the 6-m telescope of SAO RAS were performed using SCORPIO multimode focal reducer (Afanasiev & Moiseev 2005) operating in the long-slit spectroscopy mode. We used the slit of the 1 arcsec width and 6.1 arcmin length. The scale along the slit was 0.36 arcsec per pixel. The spectra were registered with EEV 42-40 CCD using VPHG550G prism as the dispersing element, which provided a spectroscopic resolution of $\delta\lambda = 13 \text{ \AA}$ (measured as FWHM of the air-glow lines) in the 3500 – 7500 \AA wavelength interval. We acquired spectra of stars and of the surrounding interstellar medium in the protocluster region at seven different slit positions; the information about all the obtained data is summarized in Table 1. Each slit passed through 2–4 stars of our interest (their names according to Fig 2 are given in parenthesis near the slit’s number). The observations with first three slit positions were performed with short exposures because the stars crossed by the slit were bright. We reduced the data using standard procedures realized in IDL pipeline developed at the SAO RAS for analysing the data acquired with SCORPIO spectrograph. The data reduction included bias subtraction, flat-field and line-curvature correction, wavelength calibration, and subtraction of night sky lines. A He-Ne-Ar lamp served as the source of the comparison spectrum for deriving the dispersion curve, and the spectrophotometric standard stars BD+25d4655 and BD+33d2642 observed at similar zenith angles before and after the object were used to calibrate the spectra. Unfortunately, spectrophotometric standard for slits 6 and 7 (stars 11, 13, 14, 18 and 20, see Fig 2) could not be observed because of weather conditions during the last night. In current analysis we were interested in relative flux calibration only, so for these spectra we used the sensitivity curve based on the data obtained during the previous night.

We analysed the spectra of stars observed in the neighbourhood of the protocluster (Fig.2) in order to determine their spectral types and, in some cases, also the luminos-

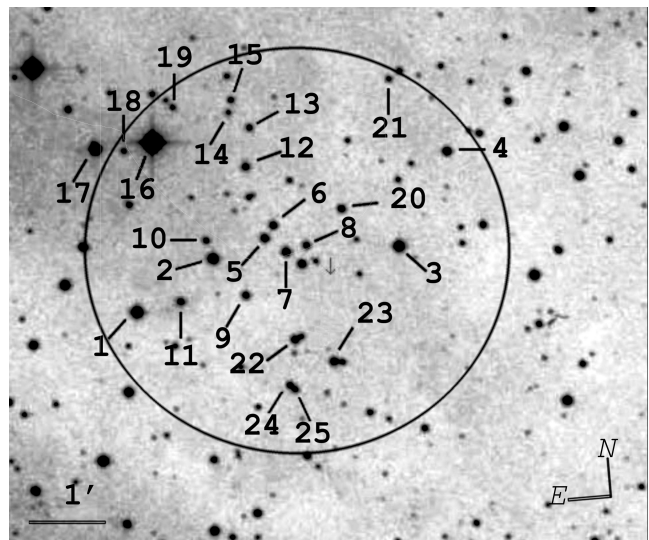


Figure 2. The optical map of the area in the direction of protocluster. The stars selected for spectroscopic study are indicated. The circle marks the same area II, as in Fig.1,bottom

ity classes. The procedure of the determination of stellar parameters consisted of three stages. At the first stage the spectral types of stars were estimated using the methods described by Gray & Corbally (2009). We used continuum-normalized spectra of MK standards from the same source. We divided the spectrum by a fifth-degree polynomial describing the form of the continuum spectrum of the object. Then we compared it with the spectra of MK standards. However, in the case of late- (M and K) type stars, whose spectra exhibit strong molecular bands, we compared the spectrum of the object with that of the standard directly without normalizing the object spectrum to the continuum. Our spectroscopic data do not allow the luminosity class to be estimated with sufficient precision except for late-type stars. Therefore we assumed, to a first approximation, that the stars studied are of luminosity class V except for star 17 (Fig.2, see also Section 4), which can be already classified as having luminosity class III. (We will later verify the luminosity class using photometric data and the distances inferred from GAIA DR2 trigonometric parallaxes.) The low spectral resolution and low signal-to-noise ratio of our observations make it also impossible to study the peculiarities of the chemical composition. We assumed in all cases that the objects studied match standard stars with no chemical anomalies. The only exceptions are stars 12 and 14 (Fig.2, see also Section 4). Thus the Ca II line in the spectrum of star 12 is significantly weaker than expected for stars of the same spectral type, whereas the spectrum of star 14 exhibits bright Eu II 6049.5 \AA line (see below).

At the second stage we determined the colour excess $E(B - V)$ based on the spectral type estimated at the previous stage and the observed colour index $(B - V)_{\text{obs}}$. We adopt the intrinsic optical and IR colour indices from Straižys (1992) and used the intrinsic colour index $(J - K)_0$ to calculate the $(J - K)_{\text{calc}}$ colour index assuming normal interstellar extinction law. If all the assumptions are true then the calculated colour index $(J - K)_{\text{calc}}$ must coincide with the observed colour index $(J - K)_{\text{obs}}$.

Table 2. Photometric parameters of stars toward the protocluster. Column 1 - number of star according to Fig.2, columns 2-7 - brightness in bands B , V , R_c , J , H , K (mag), column 8 - the trigonometric parallaxes of the stars (mas), column 9 - the corresponding distances (kpc) (without the systematic correction), columns 10 and 11 - the proper motion (mas yr⁻¹). Subscript 2 represent transformed 2MASS data.

Star #	B , mag	V , mag	R_c , mag	J , mag	H , mag	K , mag	plx, mas	D, kpc	μ_α , mas/yr	μ_δ , mas/yr
1	13.230	12.691	12.418	11.445	11.268	11.209	0.582 ± 0.029	1.72 ± 0.09	-5.040 ± 0.044	-3.130 ± 0.044
2	14.302	13.574	13.201	12.118	11.896	11.762	0.719 ± 0.016	1.39 ± 0.03	-5.575 ± 0.026	-12.665 ± 0.025
3	13.689	13.181	12.940	12.203	11.977 ₂	11.939	1.247 ± 0.016	0.80 ± 0.01	-2.157 ± 0.026	-4.524 ± 0.027
4	15.598	14.756	14.314	13.110	12.693 ₂	12.683	0.958 ± 0.023	1.04 ± 0.03	-2.544 ± 0.037	-7.455 ± 0.035
5	15.856	15.069	14.676	13.562	13.199	13.111	1.016 ± 0.023	0.98 ± 0.02	-12.359 ± 0.038	-28.540 ± 0.036
6	16.461	15.470	14.884	13.500	12.973	12.839	1.916 ± 0.026	0.52 ± 0.01	13.611 ± 0.044	14.532 ± 0.041
7	15.467	14.758	14.391	13.350	13.029	12.926	1.259 ± 0.029	0.79 ± 0.02	6.080 ± 0.035	3.213 ± 0.033
8	16.880	15.971	15.466	14.017	13.623	13.447	0.749 ± 0.036	1.34 ± 0.06	1.121 ± 0.059	7.184 ± 0.057
9	16.484	15.683	15.266	14.084	13.717	13.663	0.867 ± 0.030	1.15 ± 0.04	-3.847 ± 0.051	-15.789 ± 0.047
10	17.515	16.480	15.901	14.286	13.913	13.725	0.541 ± 0.041	1.85 ± 0.14	-2.898 ± 0.069	-6.163 ± 0.068
11	17.591	16.269	15.427	12.356	11.440	10.804	0.530 ± 0.095	1.87 ± 0.34	-5.730 ± 0.168	-4.115 ± 0.164
12	16.652	15.746	15.240	13.726	13.390	13.238	0.601 ± 0.031	1.66 ± 0.09	-0.743 ± 0.050	-2.183 ± 0.050
13	17.512	16.456	15.920	14.481	14.093	13.966	0.716 ± 0.044	1.40 ± 0.09	-1.344 ± 0.071	-4.614 ± 0.078
14	19.6	18.038	16.891	13.434	12.707	12.228	0.364 ± 0.072	2.75 ± 0.54	-2.279 ± 0.117	-3.806 ± 0.116
15	18.191	16.802	15.966	13.905	13.262	13.020	2.618 ± 0.050	0.38 ± 0.01	-7.551 ± 0.077	-40.80 ± 0.074
16	< 11.3	< 10.8	10.304	8.153 ₂	7.618 ₂	7.518 ₂	2.387 ± 0.031	0.42 ± 0.01	10.326 ± 0.046	4.836 ± 0.046
17	15.077	13.326	12.364	9.849	9.039 ₂	8.763 ₂	0.613 ± 0.031	1.63 ± 0.08	-3.116 ± 0.047	-12.758 ± 0.077
18	17.950	16.826	16.216	14.661	14.210	14.042	0.755 ± 0.052	1.32 ± 0.09	0.657 ± 0.085	-1.120 ± 0.085
19	18.730	17.360	16.436	14.204	13.570	13.337	2.680 ± 0.057	0.37 ± 0.01	2.133 ± 0.092	-10.853 ± 0.097
20	16.514	15.613	15.142	13.787	13.341	13.176	1.449 ± 0.075	0.69 ± 0.04	3.245 ± 0.130	6.295 ± 0.117
21	18.374	17.156	16.530	14.854	14.374 ₂	14.237	0.668 ± 0.065	1.50 ± 0.15	0.804 ± 0.103	-4.492 ± 0.095
22	16.383	15.415	14.893	13.414	13.026 ₂	12.949	0.654 ± 0.025	1.53 ± 0.06	-7.981 ± 0.042	-7.181 ± 0.039
23	15.724	14.999	14.627	13.536	13.224 ₂	13.183	0.831 ± 0.025	1.20 ± 0.04	1.098 ± 0.040	-2.532 ± 0.036
24	17.176	16.176	15.633	14.166	13.738 ₂	13.710	0.713 ± 0.035	1.40 ± 0.07	-2.782 ± 0.059	-1.081 ± 0.056
25	17.355	16.411	15.587	14.461	14.044 ₂	14.038	0.604 ± 0.040	1.66 ± 0.11	-3.308 ± 0.067	-0.961 ± 0.063

2.2 Photometric observations.

We carried out BVR_c photometry observations of 25 stars in the protocluster region (Fig.2) with Apogee Aspen CG-42 camera (image scale 0.37 arcsec pix⁻¹, field of view 12.6 arcmin) attached to the 60-cm telescope of the Crimean Astronomical Station of SAI MSU. The standards employed were 11–15 mag field stars with photometry errors smaller than 0.05 mag. We adopted the B , V , g' , r' , and i' -band magnitudes of these stars from the APASS catalogue² and used the colour equations from [Jordi et al. \(2006\)](#) to transform APASS data to the R_c -band filter. We performed the relative photometry of all selected standard stars with respect to each other. The accuracy of the resulting mutual calibration is better than 0.01 mag.

To obtain JHK -band data in the Mauna Kea Observatory (MKO) system, we observed our stars with ASTRON-IRCAM IR camera of the 2.5-m telescope of the Caucasian Mountain Observatory of SAI MSU ([Nadjip et al. 2017](#)). The field of view of the camera has a size of 4.6 arcmin and the image scale is 0.27 arcsec pix⁻¹. The standards employed were field stars fainter than 10 mag whose 2MASS magnitudes have errors smaller than 0.05 mag. We transformed the 2MASS data to MKO magnitudes using the colour equations from [Leggett et al. \(2006\)](#). Observations were performed using the dithering method, with the telescope shifting between individual frames by 3×4 arcsec. Each frame was corrected for non-linearity, dark current and flat field. We reduced both optical and IR frames using aperture photometry technique and standard astrometry.net ([Lang et al. 2010](#)) and photutils³ software suites. We chose the aperture size to be $\sim 2 \times \text{FWHM}$ (~ 2 arcsec). In Table 2 (columns

2–7) we present the results of our photometry of the stars marked in Fig.2. The accuracy of BVR_c -band photometry is better than 0.03 mag for stars brighter than 17.5 mag with the error amounting to 0.1 mag for 19-mag stars. The accuracy of JHK -band photometry is better than 0.02 mag. Stars 16 and 17 (see Section 4) proved to be too bright for ASTRONIRCAM, and we therefore use transformed 2MASS data for these objects. We could not acquire H -band photometry for some of the stars. In these cases we also used transformed 2MASS data (marked by subscript index ‘2’ in the Table 2). Columns 8–11 give the trigonometric parallaxes of the stars, the corresponding distances, and the proper motions of stars according to GAIA DR2 data.

2.3 Archival data

In this study we also use G , BP and RP band photometric data, colour excesses $E(BP - RP)$, trigonometric parallaxes, and proper motions from GAIA DR2 catalogue. We also applied the systematic correction to trigonometric parallaxes, which we assumed to be equal to +45 microarcseconds as estimated, e.g., from open clusters ([Yalalyeva et al. 2018](#); see also [Groenewegen 2018](#)). The exact value of this correction is not very important for the distances considered, 1.5–2 kpc: its relative contribution does not exceed 8–10 per cent.

3 ANALYSIS OF GAIA DR2 DATA FOR STARS SEEN TOWARD THE MOLECULAR CLOUD.

We use the data of GAIA DR2 catalogue to study optical objects in star-forming regions located in the cometary molecular cloud, namely, in the region of vdB 130 cluster and the protocluster (Fig.1, bottom).

² VizieR On-line Data catalogue:II/336

³ <https://photutils.readthedocs.io/en/stable/>

3.1 The open cluster vdB 130.

The vdB 130 cluster was initially identified by Racine (1968, 1974) as a compact group of B-type stars with a size of about 6 arcmin. In Paper I we analysed UCAC4 proper motions of stars in this region and found that the proper motions of 44 of 175 stars located inside the 6-arcmin radius region centred on $\alpha_{2000} \sim 20^{\text{h}}17^{\text{m}}48^{\text{s}}$, $\delta_{2000} \sim 39^{\circ}21'00''$ differ by less than 6 mas yr^{-1} (see fig. 3 and table 2 in Paper I). However, recall that vdB 130 is located in the Cygnus arm and is observed in the direction of Galactic longitude of $l \sim 77^{\circ}$. Therefore the stellar proper motions due to differential rotation of the Galaxy vary slightly with distance. That is why we decided to identify cluster members based on the proximity of not only the GAIA DR2 proper motions but also of GAIA DR2 trigonometric parallaxes.

Top panel in Fig. 3 show the CMD ($BP-RP$) – G for all stars in the 6-arcmin cone region (see Paper I) centred on $\alpha_{2000} \sim 20^{\text{h}}17^{\text{m}}51^{\text{s}}$, $\delta_{2000} \sim 39^{\circ}21'06''$. In this region there are 3370 GAIA DR2 stars. However, stars of the Cyg OB1 association also project onto this area. Central panel on Fig. 3 shows GAIA DR2 parallaxes vs. G -band magnitudes for all stars observed in this area. The stars in the narrow parallax interval from 0.5 to 0.7 mas (i.e., with distances ranging from 1.5 to 2.0 kpc) are marked by dark blue dots, with appropriate error bars. The bottom panel in Fig. 3 shows the two-dimensional proper-motion diagram for selected stars with close parallaxes. Probable cluster members with close parallax and proper motion values are marked by red dots; proper motions errors are also shown. Note that the proper motions differ by no more than 1 mas yr^{-1} from the centroid of proper motions. Probable cluster members and stars with close parallaxes are also shown on top panel of Fig. 3.

The parallax interval selected above corresponds to the distance interval from 1.5 to 2 kpc, which agrees well with the IR-data based cluster distance estimate reported in Paper I. In Fig. 3, bottom concentration of proper motions to the centroid with $(pmRA, pmDEC) = (-3.70 \pm 0.35, -5.00 \pm 0.30) \text{ mas yr}^{-1}$ is immediately apparent, and this agrees well with our results based on UCAC4 catalogue (Paper I) and on an appreciably smaller number of stars.

The proper-motion centroid in the Galactic coordinate system is located at $(pmL, pmB) = (-6.20 \pm 0.33, +0.20 \pm 0.33) \text{ mas yr}^{-1}$. The cluster obviously moves predominantly along the Galactic plane with residual velocity of about -8 km s^{-1} , i.e., toward the Galactic center (after subtracting the contribution of differential rotation and solar motion in accordance with the rotation curve based on maser sources, see Rastorguev et al. 2017). Note that stars which were selected based on the proximity of their parallaxes and proper-motion components lie along the apparent main sequence in the colour–magnitude diagram (CMD) (Fig. 3, top). Thus this fact further corroborates the existence of a stellar cluster in this region.

These 68 stars can be considered to be probable members of vdB 130 cluster inside a 12-arcmin sized area centred at the location mentioned above (see Table 3). These stars are identified using GAIA DR2 data based on their positions on the CMD, closeness of their proper motions (within 1 mas yr^{-1} of the mean value compared to 3 mas yr^{-1} when identified using UCAC4 catalogue) and parallaxes (lying in

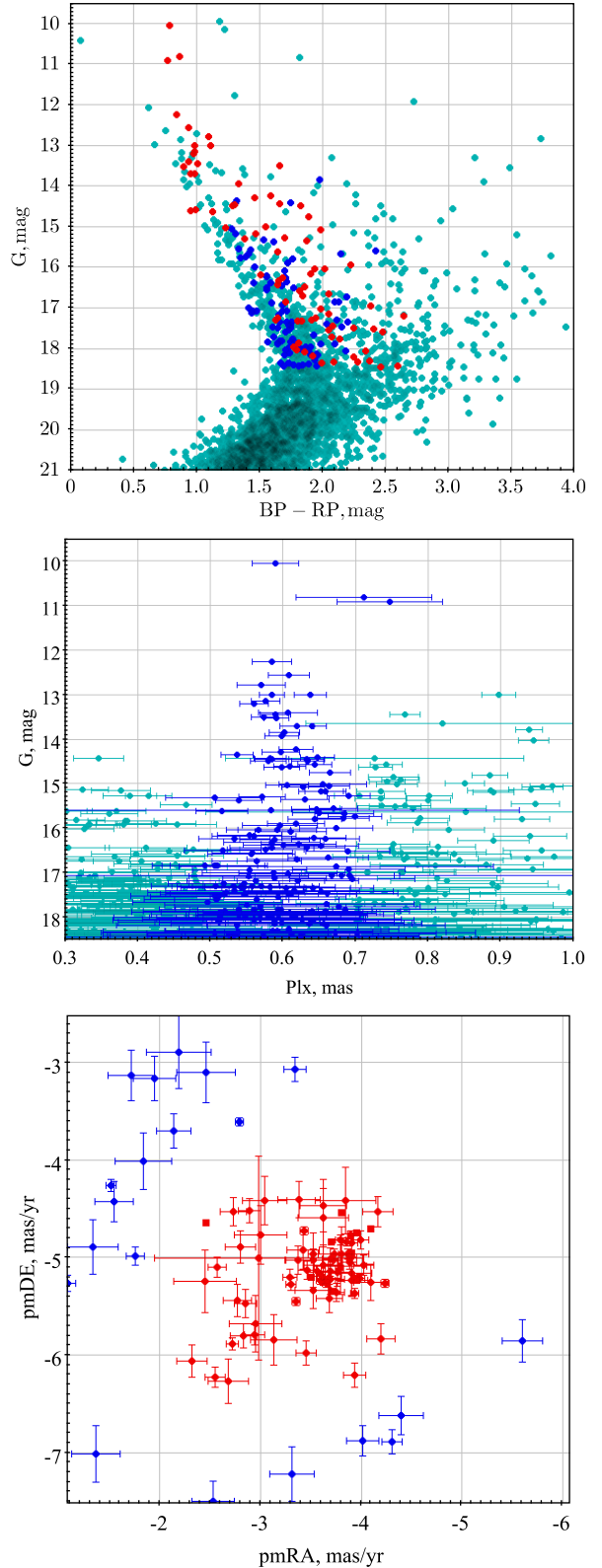


Figure 3. Top panel: ($BP - RP$) – G colour-magnitude diagram for all stars in the direction of the vdB 130 cluster. Central panel: GAIA DR2 parallax (with systematic correction of $+0.045 \text{ mas}$) – G magnitude diagram. Stars with DR2 parallaxes from 0.50 to 0.70 mas are marked by blue. Bottom panel: two-dimensional proper motion diagram for stars with close parallaxes. Probable cluster members selected both by parallaxes and proper motions are marked by red. Both selections are also marked on top panel.

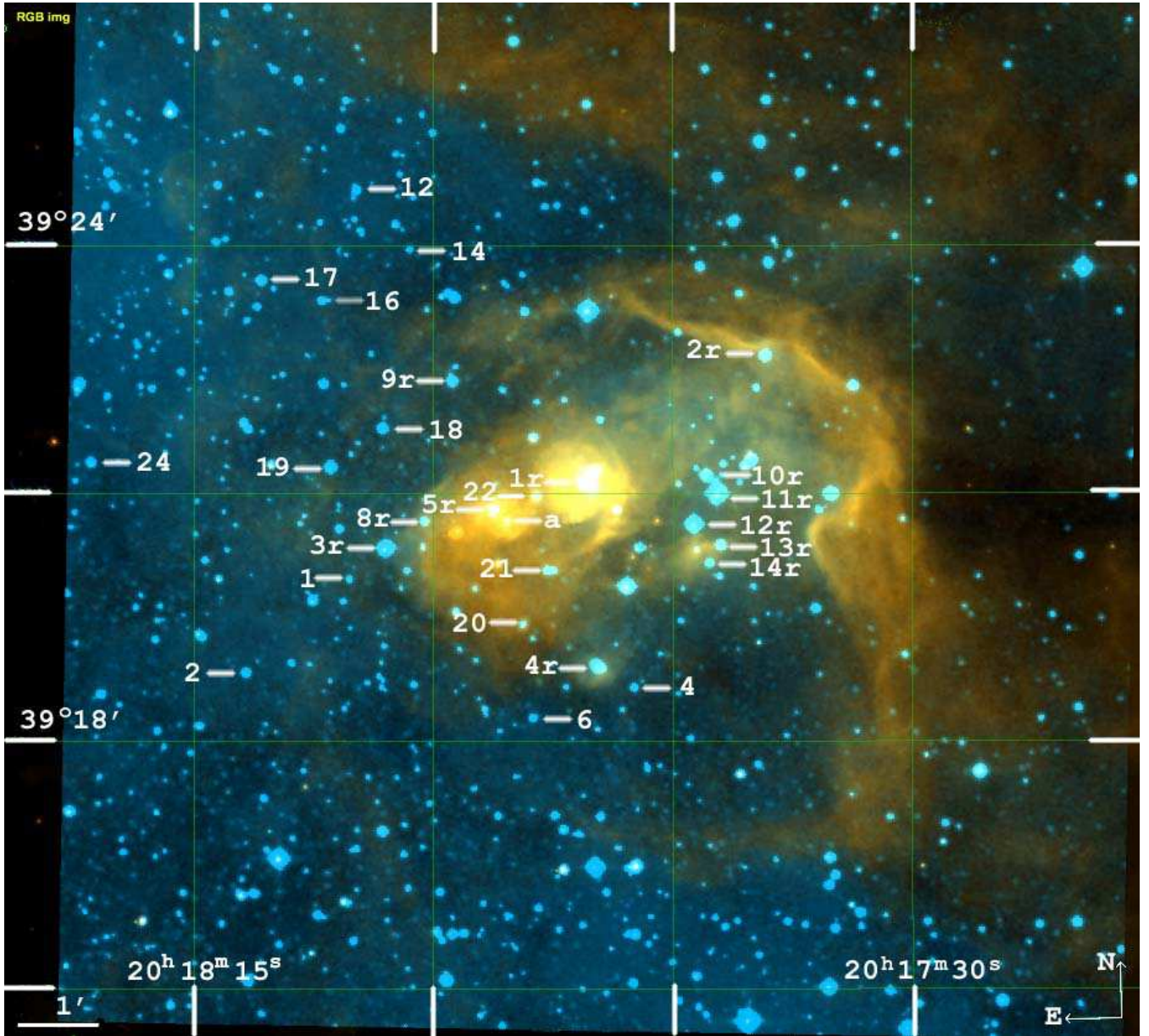


Figure 4. Superimposed images of the blue optical (F-DSS) and red IR ($8\ \mu\text{m}$ *Spitzer*) maps of the area toward the vdB 130 cluster. Also shown are the numbers of those cluster stars which have been selected from both catalogues UCAC4 and GAIA DR2 (see section 3.1 for details). The stars that initially identified by [Racine \(1974\)](#) are marked by the letter ‘r’.

the interval from 0.50 to 0.70 mas). Note that new population of the cluster contains 12 out of 14 stars (except 6r and 7r) initially identified [Racine \(1974\)](#) based exclusively on analysis of their spectra and photometry. These stars are marked by the letter ‘r’. Only 15 out of the remaining 36 stars from table 2 in Paper I met the parallax proximity selection criterion. The missing numbers in the interval from 1 to 36 correspond to the UCAC4 stars that failed to meet the selection criterion based on GAIA DR2 data. The remaining stars are identified based on GAIA DR2 data exclusively and have numbers ranging from 37 to 72. In Fig.4 are marked all stars that meet all the selection criteria based on both catalogues. The 68 GAIA DR2 stars mentioned above are most likely members of the rather compact young cluster vdB 130 with a sky-plane diameter of about 6 pc.

In Table 3 we provide a new list of cluster members extended mostly by including faint objects. Columns 1 gives source identifier in GAIA DR2 catalogue; columns 2–3 give the J2000.0 equatorial coordinates; columns 4–5, the parallaxes, uncorrected for systematical error, and appropriate random errors; columns 6–9, the proper-motion components along both coordinates with their errors; column 10, the G -band magnitudes; column 11, the $BP - RP$ colour indices, column 12, the corresponding distances and the last column, the star numbers in the cluster. Magnitudes G and colour indices $BP - RP$ are rounded to reflect real photometric precision.

Most of the stars with close proper motions (see Fig.3, bottom) lie in a rather broad line-of-sight distance interval, from about 1.5 to 2.0 kpc. Such an elongated shape of the

Table 3. The new list of the cluster vdB 130 members

Source ID	RA (J2000)	DEC (J2000)	Plx mas	e_Plx mas	pmRA mas/yr	e_pmRA mas/yr	pmDE mas/yr	e_pmDE mas/yr	G mag	BP-RP mag	Dist kpc	N
2061381510912036736	20 17 45.3942	39 22 50	0.4611	0.1158	-3.380	0.206	-4.408	0.191	17.520	2.412	2.07	37
2061377014100944000	20 18 00.4084	39 17 21	0.4658	0.1457	-3.628	0.229	-4.465	0.272	18.078	1.858	2.06	38
2061474591441143552	20 18 13.7550	39 24 57	0.4660	0.0937	-3.426	0.161	-4.922	0.192	17.548	2.051	2.04	39
2061471159769307008	20 18 20.1225	39 20 49	0.4739	0.0768	-2.728	0.131	-4.533	0.143	17.245	1.651	2.00	40
2061380484434531072	20 18 02.3379	39 20 30	0.4766	0.1087	-4.098	0.170	-5.257	0.183	17.450	2.081	2.00	41
2061474801901596928	20 18 10.9328	39 25 22	0.4865	0.0854	-4.195	0.143	-5.833	0.152	17.310	1.804	1.96	42
2061380686280218240	20 17 52.6544	39 21 09	0.4919	0.1657	-3.806	0.275	-4.964	0.276	18.196	2.253	1.98	43
2061380170883177472	20 17 43.5947	39 19 41	0.4936	0.1857	-3.849	0.299	-4.419	0.343	18.324	2.091	1.99	44
2061474355224990080	20 18 09.9918	39 22 23	0.5014	0.0762	-3.369	0.133	-5.029	0.143	17.236	1.948	1.90	45
2061380621873493376	20 17 55.3558	39 20 37	0.5088	0.0790	-3.684	0.127	-5.422	0.141	16.946	2.386	1.87	a
2061471430341784704	20 18 15.8012	39 22 27	0.5095	0.0444	-3.293	0.071	-5.200	0.081	16.158	1.912	1.86	46
2061381034190368256	20 17 41.9580	39 20 21	0.5156	0.0201	-3.951	0.030	-4.747	0.031	13.204	0.981	1.84	13r
2061474561383424000	20 18 12.7681	39 24 14	0.5158	0.1534	-3.523	0.275	-5.025	0.253	18.056	2.347	1.89	47
2061380415715060352	20 17 55.9067	39 20 07	0.5176	0.0942	-4.163	0.147	-4.529	0.175	17.194	2.645	1.85	48
2061380617558827520	20 17 53.1780	39 20 17	0.5190	0.1136	-3.527	0.179	-5.334	0.187	17.597	2.481	1.86	49
2061380003398199424	20 17 49.7267	39 18 07	0.5208	0.0439	-3.887	0.072	-5.052	0.077	16.031	1.944	1.82	50
2061380553146297728	20 18 01.4642	39 20 54	0.5243	0.1177	-3.620	0.189	-5.081	0.203	17.772	2.138	1.84	51
2061381102909847424	20 17 42.8620	39 21 11	0.5256	0.0331	-3.794	0.053	-4.819	0.053	12.776	1.099	1.81	10r
2061380381355314432	20 18 01.6577	39 20 02	0.5258	0.0324	-3.900	0.050	-5.001	0.053	15.291	1.389	1.81	52
2061381613991824256	20 17 56.7649	39 23 28	0.5303	0.6052	-2.980	1.030	-5.007	1.049	18.443	2.464	2.16	53
2061381343428026112	20 17 39.2038	39 22 38	0.5307	0.0194	-3.803	0.034	-4.538	0.031	13.145	0.990	1.79	2r
2061380037757937280	20 17 53.7773	39 19 13	0.5312	0.0532	-3.458	0.092	-5.131	0.097	16.479	1.862	1.79	54
2061381034190366208	20 17 42.6727	39 20 07	0.5346	0.0243	-3.981	0.050	-5.212	0.041	14.494	1.289	1.78	14r
2061471469006956032	20 18 20.3443	39 21 58	0.5368	0.0901	-2.800	0.153	-4.895	0.168	17.325	1.839	1.79	55
2061380656233230848	20 17 56.1791	39 20 46	0.5392	0.0237	-3.857	0.037	-4.843	0.041	14.443	1.664	1.76	5r
2061380514477932928	20 18 06.4481	39 21 17	0.5395	0.0269	-3.562	0.043	-5.140	0.047	12.252	0.845	1.76	19
2061380587513749888	20 18 03.2004	39 21 45	0.5404	0.0176	-3.501	0.028	-5.208	0.031	13.013	0.988	1.76	18
2061379964723777024	20 17 55.7345	39 18 18	0.5409	0.1486	-3.794	0.263	-5.090	0.293	18.310	2.380	1.81	56
2061380342680907136	20 17 57.3517	39 18 57	0.5432	0.0476	-3.750	0.078	-5.356	0.092	16.255	1.690	1.75	57
2061380312635856256	20 17 47.0403	39 20 19	0.5447	0.0204	-3.700	0.030	-4.843	0.036	13.449	1.009	1.74	58
2061381102909847296	20 17 42.1893	39 20 58	0.5452	0.0314	-3.865	0.047	-4.96	0.050	10.052	0.788	1.74	11r
2061474458304208512	20 18 10.8129	39 23 33	0.5456	0.0168	-3.637	0.028	-5.231	0.030	13.523	0.901	1.74	17
2061381068550105984	20 17 44.6201	39 21 05	0.5473	0.0538	-3.693	0.085	-5.013	0.109	16.046	2.022	1.74	59
2061381613991258880	20 17 57.4966	39 24 00	0.5474	0.1533	-3.619	0.253	-4.596	0.297	18.319	2.280	1.79	60
2061471400287485184	20 18 12.9841	39 21 36	0.5479	0.1228	-3.043	0.220	-4.412	0.248	17.949	1.772	1.77	61
2061380931111151360	20 17 42.0249	39 19 58	0.5506	0.0514	-3.998	0.082	-4.824	0.088	15.935	2.225	1.73	62
2061380450074795392	20 18 00.5606	39 20 38	0.5523	0.0256	-3.437	0.038	-4.731	0.045	14.286	1.465	1.72	8r
2061380243916371712	20 17 52.8373	39 20 02	0.5533	0.0233	-4.097	0.035	-4.704	0.036	13.935	1.337	1.72	21
2061379934678718976	20 17 53.7659	39 18 15	0.5539	0.0250	-4.239	0.041	-5.268	0.042	14.627	1.130	1.72	6
2061377529497025024	20 18 05.2786	39 19 56	0.5604	0.0290	-3.931	0.045	-5.373	0.050	15.027	1.235	1.70	1
2061474831956073088	20 18 06.8633	39 25 08	0.5620	0.0680	-3.678	0.118	-5.212	0.129	17.031	1.988	1.70	63
2061377254619104640	20 18 11.7472	39 18 48	0.5621	0.0402	-3.909	0.063	-4.847	0.071	13.411	0.940	1.70	2
2061380759312448384	20 17 58.8207	39 22 19	0.5631	0.0287	-3.730	0.044	-4.961	0.053	12.567	0.942	1.69	9r
2061381343428026496	20 17 40.8205	39 23 23	0.5641	0.0225	-3.606	0.036	-5.180	0.038	14.620	0.954	1.69	64
2061380553154011008	20 18 02.0406	39 21 18	0.5655	0.0911	-3.900	0.158	-5.233	0.169	17.479	2.250	1.70	65
2061380690592977280	20 17 50.3958	39 21 05	0.5732	0.0231	-3.894	0.035	-4.772	0.039	14.234	1.593	1.66	1r
2061376739215221888	20 18 4.8007	39 16 10	0.5737	0.0683	-2.854	0.114	-5.477	0.141	16.705	1.842	1.67	66
2061471258541187840	20 18 21.4792	39 21 21	0.5738	0.0237	-3.654	0.039	-5.264	0.042	13.709	0.986	1.66	24
2061377495137275520	20 18 13.4588	39 19 56	0.5827	0.0297	-3.518	0.046	-4.966	0.051	15.078	1.991	1.64	67
2061380858078916608	20 17 59.0624	39 23 24	0.5857	0.0334	-3.726	0.053	-5.022	0.058	15.355	1.873	1.63	68
2061380106477418880	20 17 47.4214	39 18 37	0.5874	0.0241	-3.353	0.038	-5.456	0.042	14.453	1.310	1.62	4
2061474733182122240	20 18 04.8118	39 24 38	0.5886	0.0220	-3.780	0.036	-5.118	0.039	14.492	1.825	1.62	12
2061380205240289152	20 17 49.7836	39 18 53	0.5924	0.0226	-3.955	0.035	-5.222	0.043	13.000	1.119	1.61	4r
2061377288978841472	20 18 14.5332	39 19 14	0.5950	0.0202	-3.727	0.030	-5.344	0.034	13.706	0.955	1.60	69
2061474423944472960	20 18 07.0185	39 23 18	0.5985	0.0230	-3.596	0.039	-5.232	0.042	14.574	0.993	1.59	16
2061380037757937152	20 17 54.3807	39 19 23	0.6077	0.0309	-3.298	0.048	-5.274	0.057	15.179	1.472	1.57	20
2061471121103942016	20 18 16.4107	39 19 42	0.6143	0.1642	-3.003	0.258	-4.766	0.296	18.183	1.927	1.62	70
2061380651920483712	20 17 56.4076	39 20 43	0.6153	0.1200	-3.901	0.199	-5.158	0.224	17.711	2.074	1.59	5r
2061380995516899584	20 17 37.6178	39 20 11	0.6161	0.1738	-3.683	0.311	-4.995	0.305	18.464	2.387	1.62	71
2061380518794267776	20 18 07.0410	39 21 41	0.6175	0.0556	-4.027	0.096	-5.075	0.105	16.653	2.049	1.55	72
2061378663368413440	20 17 39.6536	39 17 41	0.6197	0.0282	-3.897	0.044	-4.966	0.046	14.759	1.890	1.54	73
20613817514302345040	20 17 44.0534	39 24 13	0.6274	0.1520	-2.946	0.257	-5.679	0.290	18.352	1.999	1.58	74
2061474698822384256	20 18 01.4864	39 23 55	0.6461	0.0300	-3.691	0.052	-5.138	0.053	15.282	1.702	1.48	14
2061381137269500016	20 17 42.6726	39 21 53	0.6503	0.0863	-3.766	0.136	-5.145	0.146	17.142	2.048	1.49	75
20613811372691972992	20 17 43.6988	39 21 47	0.6604	0.1344	-4.274	0.209	-4.525	0.216	17.734	2.189	1.49	76
2061380484434528384	20 18 03.0200	39 20 18	0.6671	0.0934	-3.698	0.145	-5.220	0.150	10.819	0.870	1.46	3r
2061381029874009088	20 17 43.6459	39 20 36	0.7016	0.0722	-2.887	0.111	-4.517	0.126	10.923	0.772	1.38	12r
2061380621873495424	20 17 53.5368	39 20 56	0.6549	0.0605	-2.941	0.098	-5.793	0.102	15.008	1.554	1.53	22

cluster in the line-of-sight direction can be explained entirely by random errors of GAIA DR2 trigonometric parallaxes, which amount to 3–5 per cent even for the brightest stars, translating into 50–80 pc in linear measure at the average distance of about 1.7 kpc, and increase to 20–30 per cent for faint stars (see Fig. 5, red symbols). Note in this connection that apparent radial extent due to parallax errors is typical for many open clusters located at a distance about 1.5–2 kpc and more when based on GAIA DR2 parallaxes. This is immediately apparent from Fig. 5 that even for bona fide members of old open cluster NGC 188, selected on the base of CMD, parallaxes and proper motions criteria (blue symbols), located at a distance of about 1.5 kpc, relative errors of GAIA DR2 parallaxes amount to 3–5 per cent for bright stars and increase to ~ 20 per cent for faint members of this cluster. The relative error of trigonometric parallaxes evidently increases with distance.

3.2 The age of embedded cluster vdB 130 and the extinction law.

Previously, we estimated the age of the vdB 130 cluster to be within 5–10 Myr (see Paper I) based on *BVJHK* photometry and the theoretical isochrone fitting on the CMD. However, it should be noted that determining the age of young embedded clusters presents significant difficulties both because of the differential extinction and the differences in the extinction law on the way to different members of the cluster, associated with the physical properties of the dust local to the cluster. Stars inside the cluster are shifted on the CMD along the axes of colours and magnitudes relative to their ‘true’ positions. Moreover, for some stars this shift occurs along the lines $\Delta M_V - \Delta(B - V)$ of different slopes and lengths due to differences in the extinction law. For this reason, the standard procedure for applying theoretical isochrone fitting technique to the CMDs of such clusters cannot in principle give reliable results. Even if there is a good

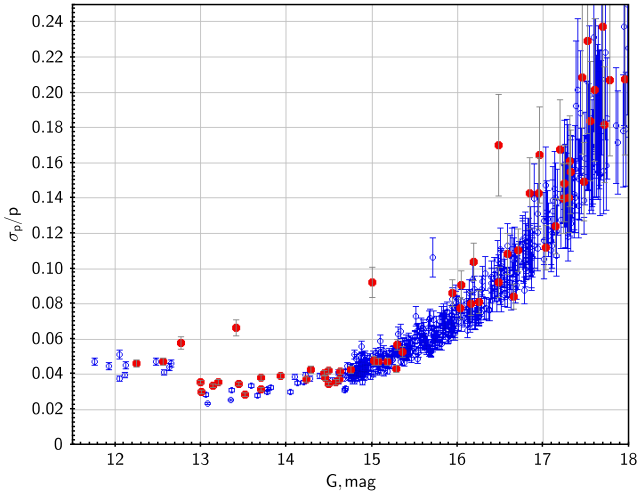


Figure 5. Dependence of the relative error of GAIA DR2 trigonometric parallaxes on the G-band magnitude for members of the vdB 130 (red) and NGC 188 (blue) open clusters.

estimate of the distance taken from the GAIA DR2 trigonometric parallax. Therefore, our age estimate published in Paper I can be considered as a preliminary.

To estimate the age of the cluster vdB 130, we used the results of spectral classification of 8 members of the cluster (1r, 3r, 4r, 5r, 11r, 12r, 19, 22), performed using data on the spectral energy distribution (SED) from [Tatarnikova et al. 2016](#). All these stars belong to spectral classes B1, B1/B2, B2/B3, B5, B5/B6 (in half of the cases neighboring spectral classes are allowed). The normal colours and absolute values for stars of these spectral classes were taken from [Pecaut & Mamajek \(2013\)](#) supplemented by Mamajek list⁴. Estimates of colour and magnitude errors were made using original data on calibration stars presented by Mamajek on the web-page⁵. The positions of stars of spectral classes B1, B2, B3, B5, B6 are indicated on diagram $M_V - (B - V)_0$ (see Fig.6).

The brightest star 11r has a spectral class B1. Based on its position on CMD, the cluster is not older than ~ 10 Myr. The large scatter of fainter stars along the colour axis (see, for example, Figure 4 in Paper I) even for IR data is explained not only by the differential absorption, but also by the fact that the lifetime of low-mass objects at the protostar stage can be comparable to the age of the cluster (~ 10 Myr). It can be clearly seen on the Fig.6 that in clusters with an age of 10 Myr, stars of A spectral class can still be on the pre-main sequence stage, and in the clusters with an age of 5-10 Myr – even some late B-stars. Thus, the age of the embedded cluster vdB 130 is no more than 10 Myr. This estimate is based on the SED analysis of eight B-stars in this cluster and is in general agreement with our preliminary estimate given in Paper I.

Even if we know more or less reliable trigonometric distance derived with the use of GAIA DR2 stellar parallaxes (true distance modulus $(m - M)_0 \approx 11.15$ mag), we can only determine the full absorption value for each star, i.e. esti-

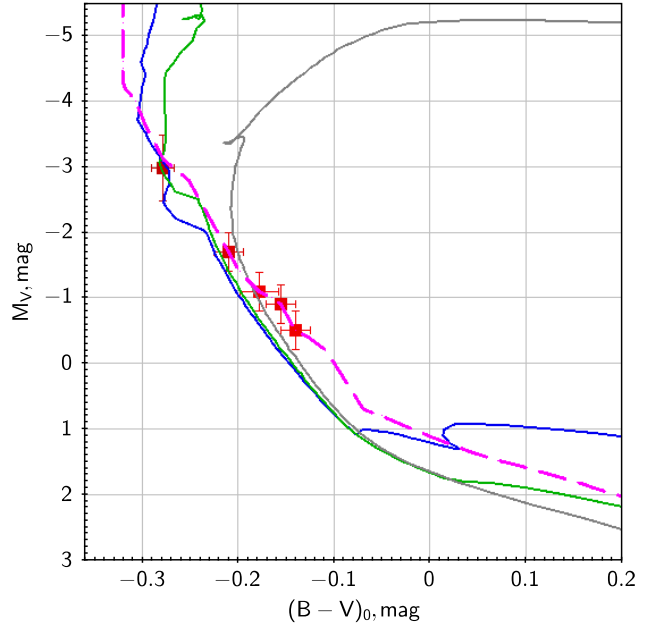


Figure 6. The colour $(B - V)_0$ – absolute magnitude M_V diagram for hot stars in the vdB 130 cluster with a spectral classification. Blue, green, and gray lines indicate Padova isochrons for ages 5, 10, and 30 Myr ([Bressan 2012](#)). Purple dashed line – calibrations of luminosities and colours of dwarf stars from Mamajek list (see text).

mate differential absorption. In the absence of any data on differential reddening, no age estimates are possible based on the position of all cluster stars on the CMD. However, for the stars with known spectral classes ([Tatarnikova et al. 2016](#)), and with absolute magnitude and colour calibrations by Mamajek mentioned above, we have attempted define the ratio $R_V = A_V/E(B - V)$, which characterizes the extinction law. In the Table 4 the absorption values of A_V and A_K , as well as estimates of R_V and $A_K/E(J - K)$ ratios for stars 1r, 3r, 4r, 5r, 11r, 12r, 19, 22 are given. The photometric data in the $BVJHK$ bands are taken from the table 2 in Paper I.

Columns 2 and 3 give the spectral class and the colour excess estimated by [Tatarnikova et al. 2016](#) using data on the spectral energy distribution (SED). Columns 4 and 7 show colour excess values $E(B - V)$ and $E(J - K)$, defined as the differences between the observed colours and colours taken from colour calibrations ([Pecaut & Mamajek 2013](#)) for the spectral classes specified in column 2. The absorption values in the bands V (column 5) and K (column 8) were estimated using obvious expressions $A_V = (V - M_V) - (m - M)_0$ and $A_K = (K - M_K) - (m - M)_0$, where true distance modulus $(m - M)_0 \approx 11.15$ mag. Finally, columns 6 and 9 give the ratios $R_V = A_V/E(B - V)$ and $R_K = A_K/E(J - K)$. From the uncertainties of colour calibrations and true distance modulus, their errors can be estimated as ≈ 0.2 . For stars with two variants of spectral classification, both values are given. Note that the colour excess values $E(B - V)$ defined by two different ways agree fairly well. It is noteworthy to note that the ratio R_V for stars 1r, 3r, 4r, 5r, 11r, 12r, 19, 22 is significantly higher than the ‘standard’ value $R_V \approx 3.1$ for the ‘conventional’ extinction law

⁴ http://www.pas.rochester.edu/~emamajek/EEM_dwarf_UBVIJHK_colors_teff.txt

⁵ <http://www.pas.rochester.edu/~emamajek/spt/>

Table 4. Members of vdB 130 cluster with spectral classification

	Sp	$E(B - V)$ (T) mag	$E(B - V)$ (PM) mag	A_V mag	R_V mag	$E(J - K)$ mag	A_K mag	$A_K/E(J - K)$ mag
1r	B1V	1.3	1.14	6.06	5.3	1.40	1.48	1.06
3r	B1V	0.9	0.86	2.85	3.3	0.47	0.51	1.06
4r	B1V/B2V	1.1	1.01/0.94	5.1/3.7	5.0/3.9	0.68/0.62	2.0/0.9	2.9/1.4
5r	B1V/B2V	1.4	1.28/1.21	6.7/5.4	5.2/4.5	1.09/1.03	2.2/1.1	2.0/1.0
11r	B1V	1.1	0.82	2.04	2.5	0.44	≈ 0	≈ 0
12r	B5V	0.5	0.68	0.80	1.2	0.36	≈ 0	≈ 0
19	B2V/B3V	0.9	0.79/0.76	3.0/2.4	3.8/3.1	0.40/0.37	0.8/0.3	2.0/0.8
22	B5V/B6V	1.4	1.25/1.23	5.0/4.6	4.0/3.7	0.92	1.3/0.9	1.4/1.0

(Cardelli et al. 1989). For stars 11r, 12r, the absorption A_K within the errors is nearly zero, which is confirmed by the relatively small absorption A_V and the unusually small value of R_V for star 12r. For stars 3r, 11r, 19, the ratio R_V can be considered as normal within the errors. The data shown in the Table 4 directly confirm the presence of abnormal absorption in the vdB 130 cluster area (see also (Tatarnikova et al. 2016)). It should be noted that for most stars, with the exception of 11r, 12r, the ratio A_K/A_V is approximately twice the ‘normal’ value ≈ 0.1 (Cardelli et al. 1989).

3.3 Protocluster region.

In the direction toward a dense condensation in the tail of the molecular cloud a compact group of class I and II protostars was found (Fig. 1, bottom, see also Paper II). While searching for optical counterparts of the protocluster we investigated the 2.5-arcmin radius area centred on the protocluster ($\alpha_{2000} \sim 20^{\text{h}}17^{\text{m}}00^{\text{s}}$, $\delta_{2000} \sim 39^{\circ}21'00''$) and found 137 GAIA DR2 stars. Like in the case of vdB 130 cluster we plotted the Hertzsprung-Russell (Fig. 7, top), parallax – G -band magnitude (Fig. 7, middle) and the two-dimensional proper-motion diagrams (Fig. 7, bottom) for stars in the direction of the protocluster. As follows from an analysis of the figures the optically observed stars making up the apparent main sequence (Fig. 7, top) span a broad interval of heliocentric distances ranging from 0.7 to 2 kpc (Fig. 7, middle). Moreover, these stars also show no appreciable concentration in the proper-motions diagram (Fig. 7, bottom) and, in our opinion, do not form a gravitationally bound group of objects.

In Paper I we proposed the following scenario of the ongoing evolution of this region (see also (Smith et al. 2010)). In the cluster area, the expanding supershell around Cyg OB1 interacts with the molecular cloud. A typical cometary shape of the cloud (an IR pillar), (see Fig. 1), is an indirect confirmation of such interaction. The wind and the UV radiation of the Cyg OB1 stars had triggered the star formation in the pillar, having resulted in the emergence of the vdB 130 cluster. The compact protocluster observed near a dense clump in the tail of the cometary molecular cloud is the next burst of star formation.

4 SPECTRAL TYPES AND COLOUR EXCESSES OF THE STARS STUDIED.

Although we could not identify a condensation of objects with close proper motions in the protocluster region, we se-

lected 25 stars for spectroscopic study. Their proper motions do not strongly differ from those of the stars of the vdB 130 cluster located in the same molecular cloud. Note that the stars studied are located within 2.5 arcmin from the protocluster centre and are projected onto the break in the star-formation filament observed there. This filament can be traced in the cometary cloud by an ensemble of several millimetre-wave sources (Motte et al. 2007). It is also described in Paper II (see fig.13 there) based on *Herschel* space telescope data.

Table 5 presents the results of our analysis of spectroscopic and photometric data for 25 stars. Column 1 gives the designation of the star according to Fig. 2; column 2, the spectral type determined in this study; column 3, the observed $(B - V)$ colour index; column 4, the intrinsic colour index characteristic of this spectral type (Straizys 1992); column 5, the $E(B - V)$ colour excess; column 6, the $(J - K)_{calc}$ colour index computed taking into account the inferred spectral type and colour excess assuming normal interstellar extinction law; column 7, the observed colour index $(J - K)_{obs}$; column 8, the absolute magnitude $(M_V)_{calc}$ determined using the distance to the object (see column 8 in Table 2) and the colour excess $E(B - V)$ assuming normal interstellar extinction law, and column 9 gives the average absolute magnitude M_V for the spectral types listed in column 2 (Gray & Corbally 2009).

As is evident from Table 5 (see columns 6 and 7), we achieved good agreement between the computed and observed colour indices $(J - K)$ for all the stars studied except two objects – stars 11 and 14 (Fig. 8). Such a significant discrepancy may be due to circumstellar envelopes surrounding these stars. Indications of circumstellar matter surrounding star 11 can also be seen in direct K -band images. Note that the distance to star 11 agrees, within the errors, with the distance to the molecular cloud, whereas according to GAIA DR2 data, star 14 must be located behind the cloud (see column 9 in Table 2). These stars exhibit certain spectral peculiarities. The DIBs can be seen in the spectrum of star 11, whereas the spectrum of star 14 shows a Eu II line (possibly blended with a Nd II line, see Fig. 8).

The star 2 (an A5-type subgiant) has the earliest spectral type among the observed stars (Fig. 8). Spectral classification of A-type stars is usually based on an analysis of Balmer lines. In our case it is very difficult to perform because the bright and highly non-uniform nebula also shines in hydrogen lines. As a result of the background subtraction, hydrogen absorption lines present in the spectrum of an A-type star may appear both stronger and weaker than in reality. However, there is another criterion for classifica-

Table 5. Physical properties of stars observed toward the protocluster. Column 1 — star numbers; column 2 — spectral types; column 3 — observed $(B - V)$ colour indexes; column 4 — intrinsic colour indexes; column 5 — $E(B - V)$ colour excesses; column 6 — calculated $(J - K)$ colour indexes; column 7 — observed $(J - K)$ colour indexes; column 8 — calculated absolute magnitudes M_V ; and column 9 — average absolute magnitudes M_V for the spectral types listed in column 2

Star	Sp	$(B - V)_{obs}$ mag	$(B - V)_0$ mag	$E(B - V)$ mag	$(J - K)_{calc}$ mag	$(J - K)_{obs}$ mag	$(M_V)_{calc}$ mag	M_V mag
2	A5 - A7V	0.73	0.15 - 0.20	0.58 - 0.53	0.39	0.36	1.1 - 1.3	1.2(A5IV)
3	F3V	0.51	0.40	0.11	0.30	0.26	3.3	3.1(F3V)
5	G2 - G5V	0.79	0.62 - 0.68	0.17 - 0.11	0.45	0.45	4.6 - 4.8	4.7(G2V)
6	K4V	0.99	1.05	≈ 0	0.66	0.72	6.9	7.1(K4V)
7	G6 - G8V	0.71	0.70 - 0.75	≈ 0	0.42	0.42	5.3	5.3(G6V)
8	G2 - G5V	0.91	0.62 - 0.68	0.30 - 0.24	0.52	0.57	4.5 - 4.6	4.7(G2V)
10	F6 - F7V	1.04	0.46 - 0.50	0.55 - 0.59	0.54 - 0.61	0.56	3.5	3.7(F6V)
11	F2 - F3V	1.32	0.36	≈ 1.0	0.77	1.55	2.0	1.9(F3IV)
12	A5 - F3V	0.91	0.30 (F0V)	0.6	0.49	0.49	2.8	2.6(F0V)
13	G2 - G5	1.06	0.62 - 0.68	0.4 - 0.34	0.56 - 0.51	0.52	4.6 - 4.7	4.79(G2V)
14	F3V?	1.56	0.40	≈ 1.2	0.87	1.21	2.2	1.9(F3IV)
15	M0 - M1V	1.39	1.44 - 1.47	≈ 0	0.89	0.89	8.9	9.2(M0V)
17	K2 - K4III	1.75	1.16 (K2III)	0.6	1.04	1.09	0.5	0.6(K2III)
18	G6 - G8V	1.12	0.75	0.37	0.62	0.62	5.1	5.3(G6V)
19	M1 - M2V	1.37	1.47 - 1.49	≈ 0	0.9	0.87	9.5	9.7(M1V)
20	K1 - K2V	0.90	0.86 - 0.91	≈ 0	0.54 - 0.59	0.61	6.4	6.3(K2V)
21	G2 - G5V	1.22	0.62 - 0.68	0.66 - 0.6	0.71	0.63	4.3 - 4.5	4.7(G2V)
22	G5 - G8V	0.97	0.68 - 0.75	0.3 - 0.23	0.54	0.47	3.6 - 3.8	3.2(G5VI)
23	F3 - F5V	0.73	0.40 - 0.44	0.33 - 0.29	0.35 - 0.26	0.35	3.7 - 3.8	3.1(F3V)

tion of A-type stars – it uses Ca II H and K lines. The fact that this is not a B-type star is evident from the absence of He I lines in its spectrum. The lack of the G-band in the spectrum and rather weak Ca I 4226 Å line indicate that we are not dealing with an F-type star.

Most of the stars (13) are of spectral types G and F. We classified G-type stars based on the depth of the G-band and intensity of the Mg I 5167, 5172, and 5183 Å lines (Fig. 8). There are a total of seven such stars and the remaining six stars are of spectral type F.

The remaining stars are of spectral type K_s and early M (see Table 5). We classified them based on the properties of MgH- and TiO-bands and the Na I 5890, 5896 Å doublet (Fig. 8). The latter, however, may be somewhat distorted because of superimposed interstellar Na I lines, but almost all such stars have small colour excesses (see column 3 in Table 5), and this effect must be weak. Note that K- and M-type stars can be rather accurately subdivided into luminosity classes V and III.

At the last stage we compared our inferred V -band absolute magnitude with the M_V estimate averaged over the spectral type and luminosity class presented by Gray & Corbally (2009). Note that we estimated the absolute V -band magnitude based on the photometric measurement, distance, and interstellar extinction. For several objects the best agreement is achieved by assuming that the star is of luminosity class IV rather than V as we initially believed. One must, however, bear in mind that the scatter of absolute magnitudes of different stars within the same spectral type and luminosity class may amount to 1 mag, which is comparable to the difference between the average M_V values for stars of luminosity class IV and V. For example, the corresponding difference for A5–A9 type stars is of about 0.8–0.9 mag.

The data from Table 5 can be used to compare the effective temperatures of stars in the protocluster region inferred from spectral types (Gray & Corbally 2009) with the temperatures provided in the GAIA DR2 catalogue. Fig. 9 shows the dependence of pointed above quantities from he-

liocentric distances to stars. It is seen from the figure that the temperatures derived using different methods agree well up to a distance of ~ 0.8 kpc. Note that the effective temperatures determined from spectra in this paper may be both lower and higher than GAIA DR2 estimates. Note also that according to our observational data the interstellar extinction toward the stars mentioned above located within ~ 0.8 kpc is close to zero (see the text below and Table 5). The difference increases with the distance (and hence with interstellar extinction) – the values of temperature provided by GAIA DR2 becomes systematically lower than our estimates. Consider, for example, stars 11 and 14, which are of spectral type F according to our estimates (Table 5). The GAIA DR2 estimates of their temperatures (about 3700 K) correspond to early M type and hence their spectra should be dominated by molecular bands. However, as is evident from Fig. 8, this is not the case. This fact is most likely indicative of insufficient account of the effect of interstellar extinction in GAIA DR2.

5 INTERSTELLAR EXTINCTION TOWARD THE MOLECULAR CLOUD.

Right panel of Fig. 10 shows the dependence of $E(B - V)$ on the heliocentric distance to stars toward the protocluster based on the data from Table 2 and Table 5. The lack of appreciable reddening toward the protocluster out to the distances of 0.6–0.8 kpc is immediately apparent. This agrees with the data from Neckel & Klare (1980) for this region and explains the agreement between GAIA DR2 effective temperatures and our temperature estimates based on spectral types within the distance limit mentioned above. In the case of normal interstellar extinction law ($R_V \approx 3.1$) extinction at larger distances increases at a rate of about 1.9 mag kpc $^{-1}$, which is in general agreement with average rate in the disk of the Milky Way galaxy (Sharov 1968). Note that star 11 is the only one to deviate significantly from this dependence. The observed $(J - K)$ colour index is much red-

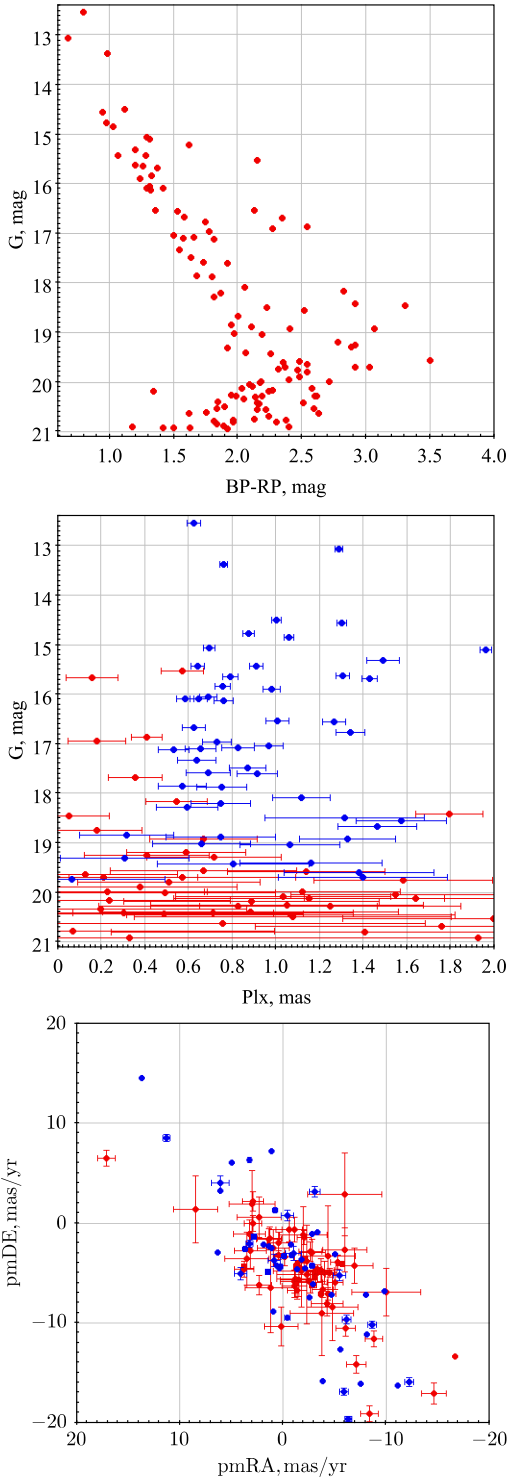


Figure 7. The same as Fig. 3 but for 137 stars in the protocluster area. The $(BP - RP) - G$ colour-magnitude diagram (top panel), parallax-magnitude diagram (middle panel) and two-dimensional proper-motion diagram (bottom panel) for stars in the direction of the protocluster. Blue symbols (middle and bottom panel) indicate the stars that form the apparent Main Sequence.

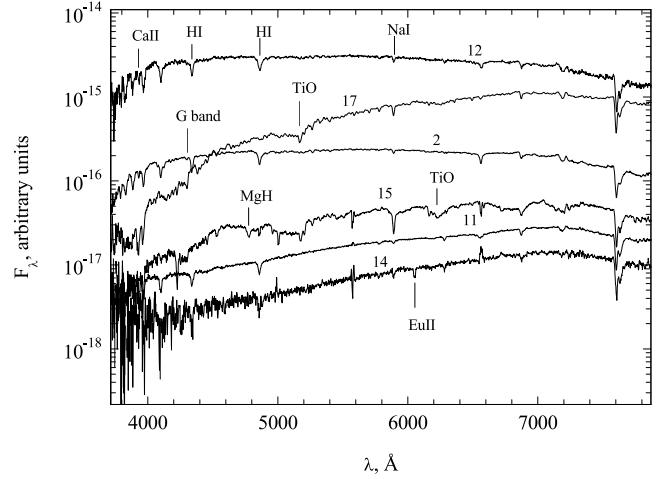


Figure 8. Examples of stellar spectra. The numbers of stars from Table 5 and spectral lines used for determining spectral classes are indicated.

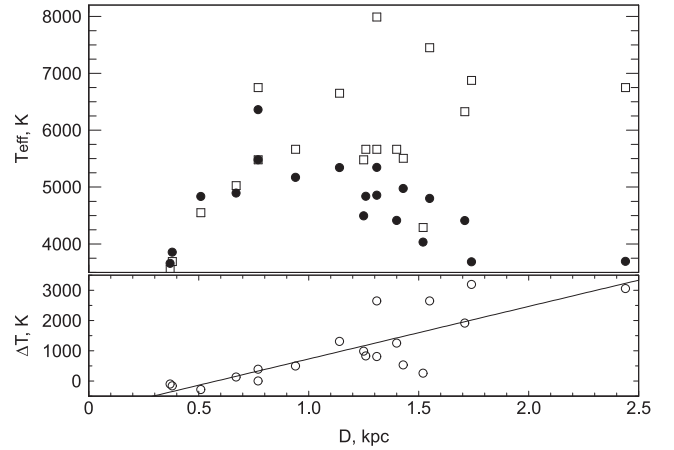


Figure 9. Distance dependence of the effective temperature derived from spectral type (the squares) and adopted from GAIA DR2 catalogue (the filled circles) — top panel, and distance dependence of the difference between these temperatures (the unfilled circles) — bottom panel.

der than calculated on the base of $E(B - V)$ colour excess under the assumption of normal extinction law (see Table 5). This object probably has a circumstellar dust shell distorting the energy distribution in the spectrum of the star. This hypothesis is supported by the fact that star 11 is a bright source on $3.6-8 \mu\text{m}$ images taken by *Spitzer* space telescope. According to Table 2, the observed colour index ($J - K$) of star 14 is also inconsistent with the colour index computed from $E(B - V)$ based on standard extinction law. However, the $E(B - V)$ is consistent with the distance to the star (see Fig. 10, right). This discrepancy may be indicative, e.g., of the presence of a circumstellar disk seen face on.

For comparison, we show in Fig. 10 (left) the dependence of $E(B - V)$ on distance for stars of the open cluster vdB 130 and field stars (with the parallaxes corrected for the systematic error). To estimate reddening values we used the spectral types and observed $(B - V)$ colour indices from (Tatarnikova et al. 2016) and adopted intrinsic colour indices from (Straizys 1992). Three stars are im-

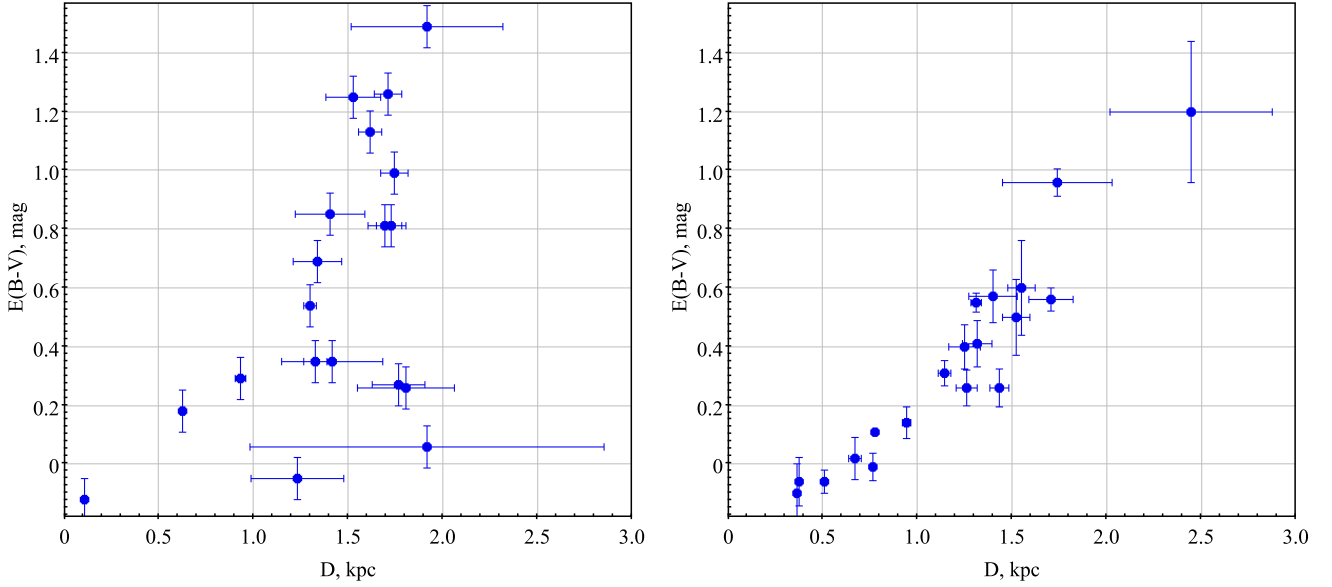


Figure 10. Dependence of the colour excess $E(B - V)$ on the distance D toward vdB 130 cluster (left) and the protocluster (right). Distances are based on GAIA DR2 parallaxes corrected for systematic error. Left panel shows not only some vdB 130 cluster members but also field stars.

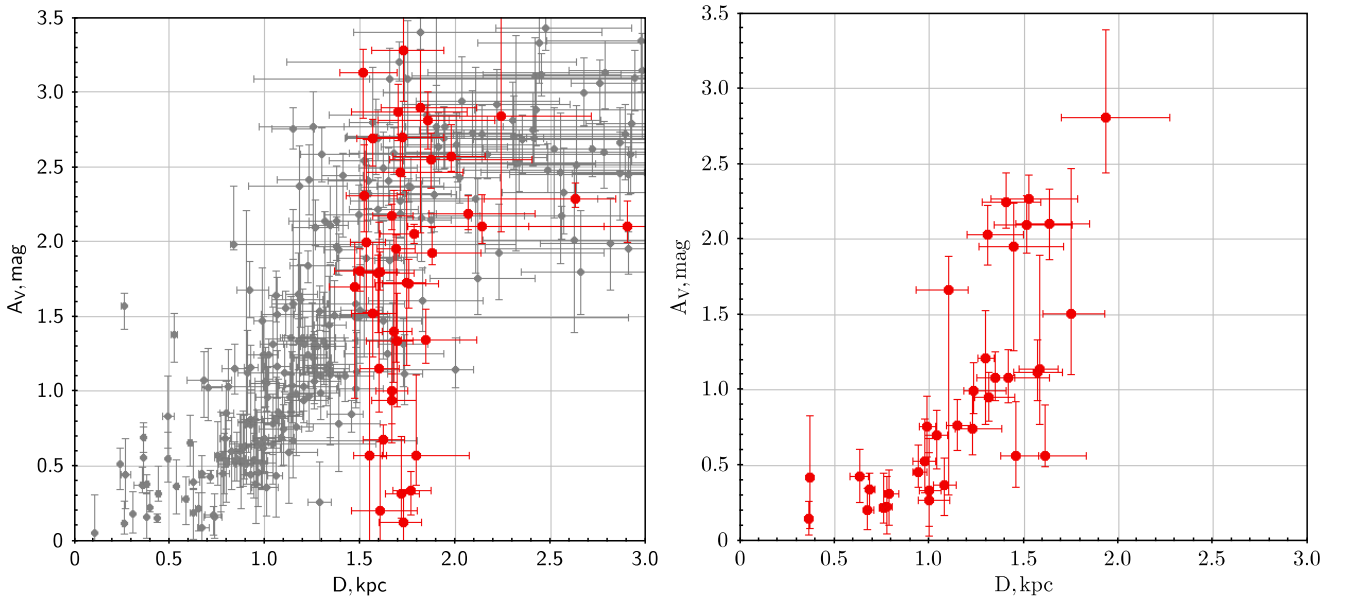


Figure 11. The same as on Fig. 10 but for the extinction A_V and distance D taken from the StarHorse catalogue (Anders et al. 2019). Left panel: vdB 130 field. Cluster members listed in the Table 3 are marked by red, and field star are marked by grey. Right panel: protocluster field. See Section 5 for details.

mediately apparent, which are located at the cluster distance of ~ 1.8 kpc and have anomalously low reddening $E(B - V) < 0.3$. According to GAIA DR2 parallaxes and proper motions, two of these stars ‘a’ and 50 are members of the vdB 130 cluster (see Table 3). Their small $E(B - V)$ colour excess may be due to the fact that these are red dwarfs (Tatarnikova et al. 2016) with magnitudes $B = 19 - 22$ mag, for which the possible $E(B - V)$ errors may amount to several tenths of a magnitude.

Like in the case of the protocluster, we can see on Fig. 10 (right panel) the lack of appreciable reddening out to a dis-

tance of about ≈ 1 kpc. For more distant stars reddening increases faster with distance than we see in Fig. 10 (right). This fact is indicative of extra extinction in the region of the young open cluster vdB 130.

By combining GAIA DR2 (G , BP , RP), PanSTARRS1, 2MASS and AllWISE photometry, Anders et al. (2019) calculated new A_V extinction values and made new Bayesian estimates of photo-astrometric distances for approximately 265 million stars brighter than $G = 18$ mag. We tried to qualitatively compare these new data taken from StarHorse catalogue by Anders et al. (2019) with our data on colour

excess and its variation along line-of-sight. Fig. 11 shows the dependence of the extinction A_V on the heliocentric distance for two fields studied in this paper: vdB 130 field of 12 arcmin size around vdB 130 cluster (left panel) and protocluster field (right panel). vdB 130 cluster members selected by CMD, distances and proper motions criteria, listed in the Table 3, are marked by red, whereas field stars are marked by grey on the left panel on Fig. 11. It is clearly seen that the extinction systematically grows with the distance up to 1.5 kpc, i.e. just to the distance of the cluster, and remains nearly constant ($A_V \sim 2.5 - 3.0$ mag) at the distances larger than 2 kpc, though with noticeable scatter. We can suppose that this 2 kpc distance marks far edge of supershell around Cyg OB1 association. As for members of vdB 130 cluster, very large scatter of their individual extinctions ($0 < A_V < 3$ mag) clearly seen on the left panel on Fig. 11 undoubtedly confirms the presence of large differential extinction inside this embedded young cluster, which is in qualitative agreement with our data in the Table 4 for stars with spectral classification (see also (Tatarnikova et al. 2016)).

Right panel on Fig. 11 shows the same dependence for protocluster area. The picture shows nearly the same behavior of extinction with the distance along line-of-sight as shown on Fig. 10 (right panel) for our data on colour excess, but with sharp increase of the extinction near $D \sim 1.5$ kpc. Additionally, the comparison of two pictures imply nearly normal extinction law with $R_V \sim 3$ (Cardelli et al. 1989) toward protocluster direction.

6 CONCLUSIONS.

In this paper we investigate two sites of star formation in the wall of the expanding supershell around the Cyg OB1 association. Both regions are associated with a cometary cloud, which is evidenced not only by the factors mentioned in Papers I and II, but also by our analysis of extinction. The region of ongoing star formation – the embedded cluster vdB 130 with an age ≤ 10 Myr, containing 68 stars – is located in the head of the cloud ‘looking’ toward the centre of the association. Whereas the burst of star formation – a compact protocluster containing at least 30 type I and II protostars – is observed in the tail of the same cloud.

We analysed the optical components in the region using the data of the GAIA DR2 catalogue and our spectroscopic and *BVRJHK* photometric observations of stars in the region. We also used our original observations to compare our data and data of the GAIA DR2 catalogue and obtained the following results:

(i) The use of high-precision GAIA parallaxes and proper motions combined with spectroscopic observations and optical and IR photometry allowed us to substantially refine the content and parameters of the open cluster vdB130. The number of members of the vdB 130 cluster previously identified using UCAC4 catalogue increased as a result of new revision of astrometric data to 68 stars with close proper motions (within 1 mas yr^{-1}) and trigonometric parallaxes (lying in the interval from 0.50 to 0.70 mas). The cluster age (less than 10 Myr) was estimated by the isochrone fitting technique applied to 8 stars with spectral classes found from SED and colour-magnitude calibrations.

(ii) We show that the relative error of GAIA DR2 parallaxes slightly increases with the distance to the object and strongly depends on G magnitude. At the distance of 1.5–2 kpc it amounts to 3–5 per cent (50–80 pc along line-of-sight) and to 20–30 per cent (300–500 pc along line-of-sight) for bright and faint stars, respectively.

(iii) The values of effective temperature provided by GAIA DR2s for stars located at distances greater than ~ 0.8 kpc toward protocluster region are systematically underestimated in comparison with the results of our optical spectroscopic observations. This appears to be because of the method used to determine effective temperatures (Andrae et al. 2018) does not properly take into account interstellar reddening.

(iv) The centroid of the proper motions of vdB 130 members in the Galactic coordinate system is located at $(pmL, pmB) \approx (-6.20 \pm 0.33, +0.20 \pm 0.33) \text{ mas yr}^{-1}$. Hence the cluster moves predominantly in the Galactic plane with a residual velocity of about -8 km s^{-1} directed toward the Galactic center (after taking into account the differential rotation and solar motion in accordance with the rotation curve of maser sources (Rastorguev et al. 2017)).

(v) We found no optical counterparts of the protocluster because our analysis of 20 stars toward the protocluster direction show no clumping in the distribution of proper motions or parallaxes. The stars studied are distributed over a broad interval of heliocentric proper motions (these stars span heliocentric distance from 0.7 to 3 kpc).

(vi) We studied the distance dependence of colour excess $E(B - V)$ and extinction A_V for field stars and cluster members toward the vdB 130, and also for protocluster based on our observations and data from StarHorse catalogue (Anders et al. 2019). The reddening is almost absent out to a distance of $\approx 0.7 - 1$ kpc. At larger distances toward the protocluster the extinction increase rate, 1.9 mag kpc^{-1} (determined assuming $R_V = 3.08$), is approximately consistent with the average rate in the Galaxy (Sharov 1968).

(vii) toward vdB 130 cluster, the extinction measured for field stars systematically increases up to 1.5 kpc, and after ~ 2 kpc remains nearly constant, with $A_V \sim 2.5 - 3$ mag. The extinction increases much steeper than toward protocluster possibly because we observe the stars through the dust and gaseous layer of a supershell around Cyg OB1. We do not exclude that the distance 2 kpc marks far edge of the supershell. For cluster members, inside the cluster large scatter of A_V values from 0 to 3 mag confirms the idea of large differential extinction.

DATA AVAILABILITY

The data underlying this article will be shared on reasonable request to the corresponding author.

ACKNOWLEDGEMENTS

The authors are grateful to Dr. Alexei Moiseev for carrying out spectroscopic observations in July 2017, and to the reviewer, Dr. Alexander Binks, for his useful comments that improved our paper.

This study was carried out using the equipment bought

with the funds of the Program of the Development of M.V. Lomonosov Moscow State University and supported by the RFBR grants (18-02-00976, 18-02-00890, 19-12-00611, 20-02-00643). Authors acknowledge the support from the Program of development of M.V. Lomonosov Moscow State University (Leading Scientific School ‘Physics of stars, relativistic objects and galaxies’). OE acknowledges the support by Foundation of development of theoretical physics and mathematics ‘Basis’.

Observations with the Russian 6-m telescope carried out with the financial support of the Ministry of Science and Higher Education of the Russian Federation.

This work is partially based on the data from the Spitzer Space Telescope operated by the Jet Propulsion Laboratory, California Institute of Technology, under NASA contract 1407, and the data from the 2MASS catalogue (University of Massachusetts, California Institute of Technology, NASA and NSF).

This work has made use of data from the European Space Agency (ESA) mission *Gaia* (<https://www.cosmos.esa.int/gaia>), processed by the *Gaia* Data Processing and Analysis Consortium (DPAC, <https://www.cosmos.esa.int/web/gaia/dpac/consortium>).

REFERENCES

- Afanasiev V.L., Moiseev, A.V., 2005, *Astron. Letters*, 31, 194
 Anders F., Khalatyan A., Chiappini C. et al., 2019, *A&A*, 628, A94
 Andrae R., Fouesneau M., Creevey O., 2018, *A&A*, 616, A8
 Bressan A., 2012, *MNRAS*, 427, 127.
 Cardelli J.A., Clayton G.C., Mathis J.S., 1989, *ApJ*, 345, 245.
 Dale J. E., Haworth T. J., Bressert E., 2015, *MNRAS*, 450, 1199
 Deharveng L., Schuller F., Anderson L.D., Zavagno A., Wyrowski F., Menten K. M., Bronfman L., Testi L., Walmsley C. M., Wienen M., 2010, *A&A*, 523, A6
 Elmegreen B. G., 1998, *Astronomical Society of the Pacific Conference Series*, 148, 150
 Elmegreen B. G., 2010, *EAS Publications Series*, 51, 45
 Egorov O. V., Lozinskaya T. A., Moiseev A. V., Shchekinov Yu. A., 2017, *MNRAS*, 464, 1833
 Brown A.G.A. et al., 2018, *A&A*, 616, A1.
 Gray R.O., Corbally C.J., 2009, *Stellar Spectral Classification*, Princeton University Press, 565.
 Groenewegen M.A.T., 2018, *A&A*, 619, A8.
 Humphreys R.M., McElroy D.B., 1984, *Astrophys. J.*, 284, 565
 Jordi K., Grebel E. K., Ammon K. A., 2006, *A&A* 460, 339.
 Lang D., Hogg D. W., Mierle K., Blanton M., Roweis S., 2010, *Astron. J.*, 137, 1782.
 Leggett S.K. et al., 2006, *MNRAS*, 373, 781.
 Motte F., Bontemps S., Schilke P., Schneider N., Menten K. M., Brogiere D., 2007, *A&A*, 476, 1243
 Nadjip A.E., Tatarnikov A.M., Toomey D.W., Shatsky N.I., Cherepashchuk A.M., Lamzin S.A., Belinski A.A., 2017, *Astrophys. Bull.*, 72, 349
 Neckel T., Klare G., 1980, *A&ASS*, 42, 251.
 Pecaut M., Mamajek E., 2013, *Aps.*, 208, article id. 9.
 Racine R., 1968, *AJ*, 73, 233
 Racine R., 1974, *Astron. J.*, 79, 945.
 Rastorguev A.S., Utkin N.D., Zabolotskikh M.V., Dambis A.K., Bajkova A.T., Bobylev V.V., 2017, *Astrophys. Bull.*, 72, 122
 Sharov A.S., 1968, *Soviet Astron.*, 7, 689.
 Schneider N., Simon R., Bontemps S., Comeron F., Motte F., 2007, *A&A*, 474, 873
 Sitnik T.G. et al, 2015, *MNRAS*, 454, 2486
 Sitnik T.G. et al, 2019, *MNRAS*, 486, 2449
 Smith N. et al, 2010, *MNRAS*, 406, 952
 Strazys V., 1992, *Multicolour Stellar Photometry*, Pachart, Tucson. (1977, Moksas, Vilnius).
 Tatarnikova A. A., Tatarnikov A. M., Sitnik T. G., Egorov O. V., 2016, *Astron. Lett.*, 42, 790
 Yalyalieva L. N., Chemel A. A., Glushkova E. V., Dambis, A. K., Klinichev, A. D. 2018, *Astrophys. Bull.*, 73, 335
 Zavagno A., Deharveng L., Comerón F., Brand J., Massi F., Caplan J., Russeil D., 2006, *A&A*, 446, 171